



MWCNT-Doped Polypyrrole-Carbon Black Modified Glassy Carbon Electrode for Efficient Electrochemical Sensing of Nitrite Ions

Md. A. Rashed^{1,2} · M. Faisal^{1,3} · Mabkhoot Alsaiani^{1,4} · S. A. Alsareii^{1,5} · Farid A. Harraz^{1,6} 

Accepted: 21 June 2021 / Published online: 6 July 2021

© The Author(s), under exclusive licence to Springer Science+Business Media, LLC, part of Springer Nature 2021

Abstract

In the present research, we have reported the applicability of multiwall carbon nanotube-doped polypyrrole-carbon black (MWCNTs/PPy-C) as a potential nitrite sensor. Sophisticated characterization tools including X-ray diffraction, X-ray photoelectron spectroscopy, Raman spectroscopy, infrared spectroscopy, and transmission electron microscopy were systematically employed to characterize the as-fabricated electrocatalyst. The electro-catalytic and sensing performance were evaluated using cyclic voltammetry (CV), linear sweep voltammetry (LSV), electrochemical impedance spectroscopy (EIS), and amperometric (*i-t*) techniques. The as-fabricated sensor electrode shows remarkable electrocatalytic activity towards nitrite ion electro-oxidation. The nitrite oxidation using the proposed catalyst follows a diffusion-controlled process with kinetic parameters having electron transfer coefficient (α) as 0.50 and the standard rate constant (k^0) as $5.488 \times 10^{-3} \text{ cm s}^{-1}$. The MWCNTs/PPy-C modified sensor electrode exhibited excellent sensitivity of $0.1558 \mu\text{A}\mu\text{M}^{-1} \text{ cm}^{-2}$ over the dynamic concentration range (0.50–10.50 mM) (for linear sweep voltammetry: LSV) and $0.1171 \mu\text{A}\mu\text{M}^{-1} \text{ cm}^{-2}$ over the concentration range (5–9500 μM) (for amperometry: *i-t* characteristics). The detection limit was calculated to be 2.30 μM and 3.06 μM ($S/N = 3$) for LSV and *i-t* technique, respectively. Furthermore, the proposed sensor electrode exhibited good selectivity towards nitrite ion detection in the existence of common interfering metal ions and biomolecules as well as demonstrated excellent operational stability, reproducibility, and repeatability. Therefore, such developed electrocatalyst demonstrates a promising sensor material for the competent detection of nitrite ions by the electrochemical method.

Keywords MWCNTs · PPy · Nitrite ions · Kinetics · Voltammetry · Amperometry

Introduction

Nitrite ion (NO_2^-) is one of the toxic inorganic substances that poses a serious threat towards food and drinking water. Nitrite is widely used as an additive for food preservation due to its antimicrobial action [1]. Besides, nitrite is commercially used in industries as a dyeing agent [2], bleach [3], and corrosion inhibitor [4]. Therefore, the widespread existence of NO_2^- in soil, water, food, and physiological systems is well known [5]. Unfortunately, numerous studies have been revealed that NO_2^- is a shocking pollutant for human health and the environment. For human being, nitrite creates severe diseases such as stomach and esophagus cancer by reacting with the dietary compound under the acidic condition of the stomach forming toxic and carcinogenic nitrosamines [6]. In addition, NO_2^- can interrelate with the blood hemoglobin resulting in methemoglobin by irreversible oxidation process, which consequently removes oxygen from the body or creates oxygen deficiency for tissues

✉ Farid A. Harraz
faharraz@nu.edu.sa

- ¹ Promising Centre for Sensors and Electronic Devices (PCSED), Advanced Materials and Nano-Research Centre, Najran University, P.O. Box: 1988, Najran 11001, Saudi Arabia
- ² Department of Chemistry, Faculty of Science, Mawlana Bhashani Science and Technology University, Santosh, Tangail 1902, Bangladesh
- ³ Department of Chemistry, Faculty of Science and Arts, Najran University, Najran, Saudi Arabia
- ⁴ Department of Chemistry, Faculty of Science and Arts at Sharurah, Najran University, Sharurah, Saudi Arabia
- ⁵ Department of Surgery, College of Medicine, Najran University, Najran, Saudi Arabia
- ⁶ Nanomaterials and Nanotechnology Department, Central Metallurgical Research and Development Institute (CMRDI), P.O. 87 Helwan, 11421 Cairo, Egypt

[7, 8]. This conversion leads to oxygen deficiency disease, especially for the infants, namely, “Blue baby syndrome” and breath shortness [9, 10]. According to the world health organization (WHO) guidelines, the dangerous level of nitrite intake in the human body is $\geq 8.7 \mu\text{M}$ [11]. Therefore, it is inevitable need to continue the nitrite concentration monitoring in food and drinking water for public health and environmental security.

In order to monitor the nitrite concentration, several analytical techniques have been applied, including spectrophotometry [12], Raman spectroscopy [13], and gas chromatography-mass spectroscopy (GC-MS) [14]. These reported techniques are considered reliable but time-consuming, costly, and need sophisticated and complicated instrumentation for proper analysis [15]. In contrast, the electrochemical method has advantages for nitrite detection from the aqueous solution even at trace concentration levels because of its high sensitivity. Moreover, this technique offers a rapid detection, high accuracy, and real-time analysis; predominantly, this technique is considered a relatively safe and environmental friendly analytical approach with fewer reagent consumption [16, 17]. The electrochemical detection of nitrite ions can be followed by either oxidation or reduction procedures. The oxidation of nitrite is favorable than the reduction process because readily reducible compound nitrate ion (NO_3^-) (the major co-existing species) cannot interfere in the anodic nitrite determination [18, 19]. In addition, the interference effect of molecular oxygen is eliminated during the detection of nitrite via the oxidation process [17–19].

The electrochemical nitrite detection has been investigated on bare or polycrystalline electrodes, such as platinum [20], gold [21], and carbon-based electrodes including carbon ceramic electrode (CCE) [22], carbon paste electrode (CPE) [23], and glassy carbon electrode (GCE) [24]. However, the electrochemical oxidation of nitrite ion using bare electrodes requires exceptionally high positive potential, and the surface of the electrode tends to be poisoned (electrode fouling) by several electroactive species during this oxidation process, consequently reduces the sensing performance [25].

The most promising approach for lowering the overpotential required during the electrochemical reaction as well as enhancing the sensitivity and selectivity is to modify the naked electrode surface using appropriate surface mediator. Concurrently, conductive polymers received much scientific and technological attention in the electrochemical sensor applications as a redox mediator with direct charge transport features [11]. A variety of conducting polymers, for example, polyaniline (PANI), polythiophene (PTh), and polypyrrole (PPy), have been widely investigated for the electrochemical sensor applications [26–29]. These conductive polymers showed good electrical conductivity with high mechanical flexibility and chemical strength. Moreover,

those conductive polymers exhibited vast effective catalytic efficiency with sole electrochemical competence [30]. Recently, PTh/ZnO, $\alpha\text{-Fe}_2\text{O}_3$ /crosslinked PANI, and PANI/SrTiO₃ nanocomposites modified GCEs have been reported by our group [31–33]. Among the conductive polymers, and because of the easy synthesis procedure, chemical and thermal stability, and high electrical conductivity, PPy is considered one of the most general intrinsic conducting polymers (ICPs) [34, 35]. However, the electrode modified with only conducting polymer may face several challenges regarding the considerable sensitivity and operational stability. In addition, high overpotential might require in the electrochemical process, and the electrode shows a low selectivity due to the interference of several common interfering species in this high overpotential regime [11].

To overcome those limitations, a relatively high conductive and large surface area containing carbon nanomaterials (porous carbon, graphene, carbon nanotubes (CNTs), etc.) can be utilized as dopant materials to fabricate nanocomposite with conductive polymer. Among carbon nanomaterials, CNTs have received significant interest after discovery by Iijima in 1991 [36]. The sp^2 hybridization of CNT makes it a promising material for different potential applications due to its unique structural and chemical features. Predominantly, multi-wall carbon nanotubes (MWCNTs) have received great attention as electro-catalyst for different types of chemical and biochemical sensor applications, because of its exceptional electrical conductivity, high chemical and mechanical durability, strong adsorption ability, and biocompatibility, and finally it provides high effective surface area [37–39]. In addition, the unique property of MWCNTs that may provide a wide potential window as well as MWCNTs could act as electron movement channel between the active surface of the working electrode and the analyte [40, 41].

Recently, conducting polymer/CNT composite materials have attracted noteworthy attention because the doped CNTs can lead to multifunctional composite materials [42]. This composite material would contain the individual properties of each component as well as provide synergistic influences, which might facilitate the sensor performance during the electrochemical sensor applications. The CNT/conductive polymer composites for nitrite ion sensor including polyaniline/carbon nanotubes [43], polyvanillin/multiwall carbon nanotubes [8], polypyrrole/SDS/functionalized multiwall carbon nanotubes [44], poly (azure A)/carbon nanotubes [45], and chitosan/carboxylate multiwall carbon nanotubes [46] have already been reported.

In the current study, we focused on the utilization of MWCNTs/PPy-C nanocomposite modified GCE for the kinetic investigation of NO_2^- oxidation reaction as well as sensing and quantifying the NO_2^- from the aqueous phase. The nanocomposite was synthesized using a simple ultrasonication technique. The synergistic coupling effect induced in

the current-developed nanostructure due to the close interaction of MWCNTs and PPy [47] could significantly enhance the catalytic property towards nitrite ion electro-oxidation. The newly developed electrocatalyst was extensively investigated using spectroscopic methods such as Fourier transform infrared spectroscopy (FTIR), Raman spectroscopy, and X-ray diffraction (XRD), X-ray photoelectron spectroscopy (XPS), and transmission electron microscopy (TEM) techniques. The kinetic investigations and sensing performance of the as-fabricated electrocatalyst were evaluated using several electrochemical tools, including cyclic voltammetry (CV), electrochemical impedance spectroscopy (EIS), linear sweep voltammetry (LSV), and the highly sensitive amperometric (*i-t*) techniques. The obtained results illustrate that the newly prepared sensor electrode provides competitive sensor performance with a wide dynamic detection range, acceptable limit of detection, and highly sensitive and selective towards NO_2^- detection. Hence, the combined properties of MWCNTs and PPy could lead to an efficient electrocatalyst for the selective detection and quantification of nitrite ion. Furthermore, the current fabricated sensor was successfully employed for the recovery NO_2^- from both tap water and deep-well water samples as a validated practical analysis route.

Experimental

Materials

Polypyrrole ~20 wt% loading, composite with carbon black (PPy-C), and multiwall carbon nanotube were purchased from Sigma-Aldrich (St. Louis, MO, USA) and Merck, Germany, respectively, and used as-received without any refinement.

Synthesis of 5%MWCNTs/PPy-C Nanocomposite

Ultra-sonication technique was simply applied for the fabrication of 5 wt% MWCNTs/PPy-C nanocomposite. A typical procedure, 3.8 g PPy-C, was mixed with 0.2 g MWCNTs. Then, the deionized water (100 ml) was added into the mixture and ultra-sonicated for 30 min using a sonication bath at ambient conditions. The resulting mixture was then filtered, followed by washing several times with deionized water and ethyl alcohol, and finally kept for 24 h in an oven for drying at 65 °C in order to get MWCNTs/PPy-C nanomaterial.

Characterization of Materials

The structural property of the as-fabricated nanocomposite was examined using a Bruker D4 Endeavour X-ray diffractometer with a radiation of $\text{Cu K}\alpha_{1/2}$, $\lambda\alpha_1 = 154.060$ pm,

$\lambda\alpha_2 = 154.439$ pm. For elemental analysis of the nanocomposite surface, XPS investigation has been performed using K-ALPHA spectrometer (Thermo Fisher Scientific, USA) with X-ray $\text{AlK}\alpha$ monochromatic radiation source (–10 to 1350 eV). The energy calibration and peak deconvolution of the narrow scan spectrum were done using XPS peak fit bundled software with a linear background. Chemical bonding of the nanocomposite samples was evaluated using Raman and FTIR spectroscopy techniques using Raman station-400 and FTIR spectrum-100 from Perkin Elmer. Raman spectra were recorded at room temperature using 60% of its 300-mW power at a radiation laser line wavelength (λ) 785 nm and an integration time 20 s. In order to investigate the surface morphology, a transmission electron microscope (TEM) was employed with a JEOL JEM-2100F-UHR field emission instrument fitted out with a Gatan GIF 2001 energy filter with 200 kV acceleration voltage and 1 k-CCD camera.

Sensor Fabrication and Electrochemical Characterization

The glassy carbon electrodes (apparent surface area = 0.071 cm^2) (BAS Inc. Japan) were used as the working electrode during the electrochemical investigation. Before use, the electrode surface was finely polished with $1.0 \mu\text{m}$ diamond paste, followed by $0.05 \mu\text{m}$ alumina slurry. An ultrasonication bath was used for cleaning the polished electrodes using ethyl alcohol and deionized water, respectively, followed by washing a couple of times with those solvents and finally dried with airflow. To modify the clean GC electrode surface, 10 mg of CNTs/PPy-C nanocomposite was nicely dispersed in 0.9 ml isopropanol and 0.1 ml of 5 wt% Nafion solution. The homogenous suspension was obtained by ultra-sonication for 30 min, followed by vortex for 15 min. To obtain an active layer, $3.0 \mu\text{l}$ of catalyst suspension was cautiously dropped onto the electrode surface ($1.5 \mu\text{l}$ in individual drop and dried at normal condition), dried in an oven at 60 °C for 30 min. After that, further $9 \mu\text{l}$ of the above suspension was dropwise added to the electrode surface as the above-mentioned process. Finally, the electrode was dried at 60 °C for 30 min in an oven and stored in N_2 atmospheric inert condition before the electrochemical investigation. For comparison, the PPy-C modified GCE was further prepared using identical procedure. A three-electrode system with a personal computer was connected to the electrochemical workstation (ZahnerZennium, Germany) and subsequently used for the electrochemical investigations. In the electrochemical studies, the active material modified GCE acted as a working electrode, whereas a KCl saturated Ag/AgCl served as a reference, whereas a Pt spiral wire was used as a counter electrode. The experiments were conducted in a phosphate buffer solution (PBS) having pH = 7.1.

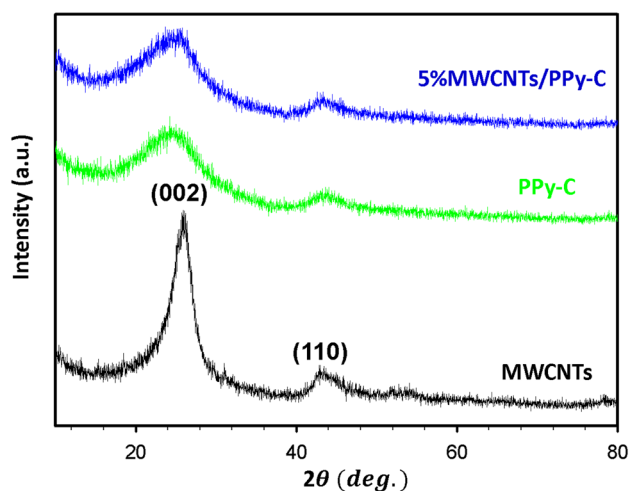


Fig. 1 XRD pattern of MWCNTs, PPy-C, and MWCNTs/PPy-C nanocomposite

Results and Discussion

Physicochemical Characterization

In order to define the structural property of the MWCNTs/PPy-C nanocomposite, XRD analysis has been carried out. Figure 1 demonstrates the XRD pattern of as-fabricated nanocomposite as well as base materials MWCNTs and PPy-C. The XRD spectrum of MWCNTs refers to two peaks at 25.9° and 43.6° corresponding respectively to the (002), and (110) of pristine MWCNTs in a good agreement with reported literature [48]. The XRD pattern corresponding to the PPy-C provides a broad characteristic peak centered at $2\theta = 24.7^\circ$ indicating the amorphous carbon material. In addition, a peak was observed at $2\theta = 43.8^\circ$, which could be indexed to the carbon (110) reflection of graphite. The reflection peak at 24.7° is slightly higher than the reported amorphous polymer of pure PPy observed at $2\theta = 24.0^\circ$ [49]. This shifting might happen in the presence of 80% amorphous carbon nanomaterials into the PPy, which shifted the peak position between MWCNTs (25.9°) and pure PPy (24.0°). Finally, the XPD pattern of MWCNTs/PPy-C nanocomposite shows two-broad peaks, centered at 25.0° and 43.6° . It is well known that the broadening of the XRD peaks reflects the decrease in the order of crystallinity. Therefore, from the above discussion, we may conclude that for MWCNTs/PPy-C nanocomposite, the amorphous character of carbon is more dominating. In addition, the position shift of the XRD peaks of fabricated nanocomposite compared to pristine MWCNTs, and PPy-C revealed the successful formation of MWCNTs/PPy-C nanocomposite.

The XPS investigation was further carried out in order to endorse the successful formation of MWCNT-doped PPy-C nanocomposite. From the survey scan XPS spectrum

(Fig. 2a), the photoemission lines are visible form of the states of core lines of carbon (C1s (ca.284 eV)), nitrogen (N1s (401 eV)), oxygen (O1s (ca. 531 eV)), Auger C KLL lines (ca. 1200 eV), and Auger O KLL lines (ca. 980 eV), which are well matched with the relevant literature for CNTs

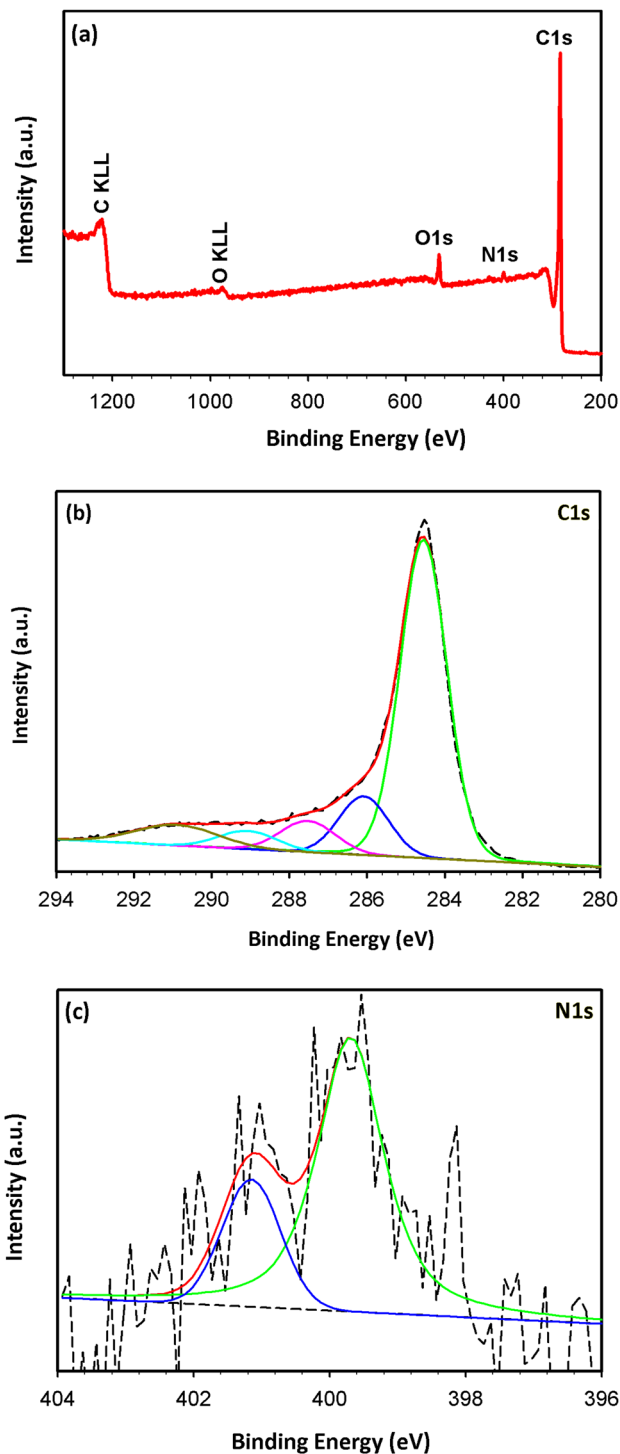


Fig. 2 XPS survey scan spectrum of (a) MWCNTs/PPy-C nanocomposite, and related fine-scan spectrum for (b) C1s and c N1s

[50]. Energy calibration was done using the reference value of C1s at 284.8 eV. After deconvolution, the C1s narrow scan spectrum provides five distinguishing peaks (Fig. 2b). The highest intensity and lowest binding energy (BE) peak at 284.5 eV are accredited to the C–C/C=C [51, 52]. The 286.1 eV BE peak is assigned to C–O (due to hydroxylate defects (C–OH)) and C–N [53]. In addition, this peak might be accredited by the imine-like (C=N), and/or polaron (=C–NH•+) due to the presence of polypyrrole (PPy) [54, 55]. Moreover, the C1s peak at 287.3 eV is attributed to the carbonyl (C=O) group and the 289.0 eV is due to carboxylic (–COOH) group [56, 57]. Finally, the highest BE peak at 290.9 eV can be associated with the π - π^* satellite, which usually found in aromatic PPy. This satellite peak was detected ca. 6.30 eV higher than the major peak of C1s, which is consistent with the reported literature [52, 55]. In the term of N1s high-resolution spectrum (Fig. 2c), the deconvolution of N1s demonstrated two components. The major peak at 399.6 eV was assigned to the characteristic pyrrolium nitrogen (-NH), and the higher binding energy peak at 401.1 eV can be attributed to the oxidized or positively charged nitrogen as polaron (C–N⁺) structure of nitrogen [57–59].

To define the chemical bonds in the fabricated nanocomposite, Raman and IR studies were conducted. Raman spectra of as-fabricated nanocomposite as well as MWCNTs and PPy-C are shown in Fig. 3a. The Raman spectra of MWCNTs demonstrate two characteristic Raman peaks for pristine MWCNTs. The peak at 1326 cm⁻¹ is ascribed to the disordered graphite, so-called Raman active D-band. The second peak placed at ca. 1690 cm⁻¹, is related to the Raman active G-band, and is ascribed to the E_{2g} mode of graphite

wall. From the literature, for CNTs, the wavenumber of the G-band position can be shifted maximum up to 1600 cm⁻¹ [59]. However, in the present study, the G-band position was observed at 1690 cm⁻¹. According to reported literature, the G-band position may move to a maximum of 1600 cm⁻¹, for materials containing sp² rings. However, for the materials containing SP² chains, the G-band would increase beyond 1600 cm⁻¹ and could extent up to 1690 cm⁻¹ [60]. In addition, an unusual and strong Raman band was detected at ca. 1940 cm⁻¹, which has been endorsed to the vibration of the 1D chain of carbon atoms [61, 62]. The Raman spectra of PPy-C show relatively similar peaks as pristine MWCNTs, with an additional peak at ca. 845 cm⁻¹, which could be associated with the polaron structure of PPy. However, this peak is shifter slightly to a lower frequency than pure PPy (at 934 cm⁻¹) [55]; this might happen due to the interaction of carbon with PPy. In addition, the broad peak ranging from 1400 to 1750 cm⁻¹ might be composed of C=C (st.) vibration and C–N (st.) vibration mode of pure PPy, which is similar to the reported literature of pure PPy [63]. However, in case of MWCNT-doped PPy-C, Raman spectrum did not show any new peak except the characteristic peaks of MWCNTs and PPy-C.

The FTIR spectra of MWCNTs, PPy-C, and as fabricated MWCNT-doped PPy-C nanocomposite are shown in Fig. 3b. The IR spectra of MWCNTs represent the vibrational bands at 1063 cm⁻¹, 1315 cm⁻¹, 1611 cm⁻¹, and 1725 cm⁻¹. The peak at 1611 cm⁻¹ corresponding to the C=C (st.) mode could arise from the carbon nanotubes sidewall [64]. The peak centered at 1725 cm⁻¹ represents to the C=O group on CNTs surface, might arise from the partial oxidation of CNTs in the existence of atmospheric oxygen. The peaks

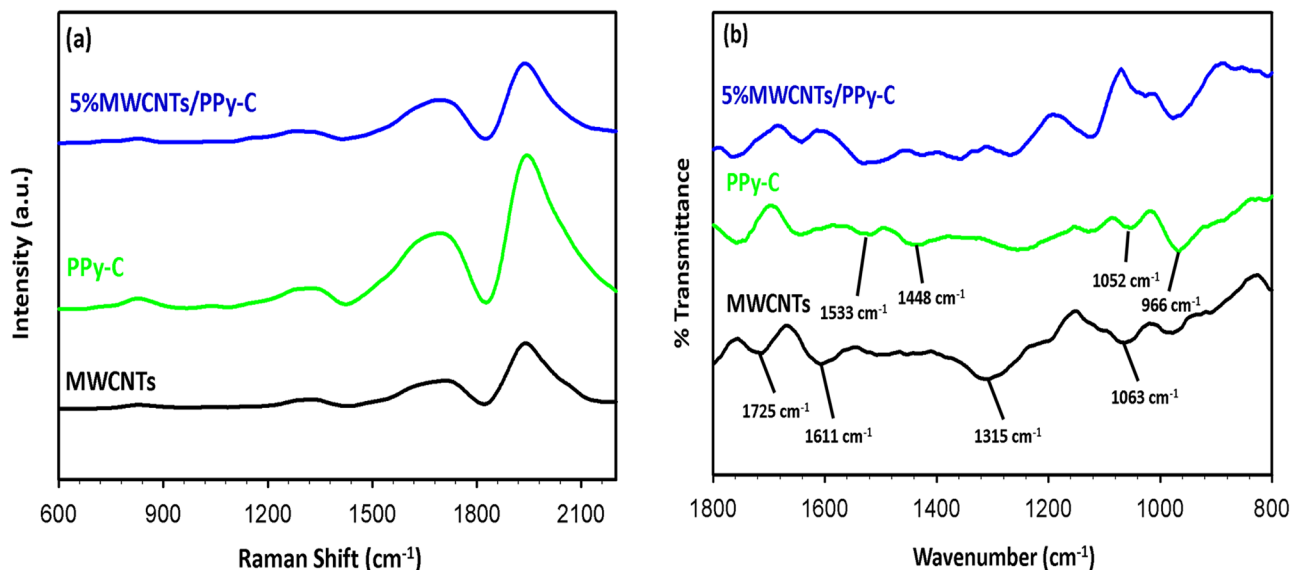


Fig. 3 Raman (a) and FTIR (b) spectrum of MWCNTs, PPy-C, and MWCNTs/PPy-C nanocomposite

at 1063 cm^{-1} and 1315 cm^{-1} represent the C–N stretching mode [65]. The FTIR spectra of PPy-C showed the characteristic bands of PPy, mainly for the deformation vibration of (a) C–H out of plane at 966 cm^{-1} and (b) C–H in plane at 1052 cm^{-1} . In addition, a peak for C–C asymmetric stretching vibration at 1448 cm^{-1} , and a peak at 1533 cm^{-1} , attributed to the C=C/C–C stretching vibration of PPy rings. These results are consistent with the earlier reports on polypyrrole [47, 66]. The major characteristic peaks of PPy-C and MWCNTs have closely resembled in the MWCNTs/PPy-C spectrum. However, slight peak shifting was observed, indicating the interaction between MWCNTs and PPy-C nanomaterials.

The surface morphology of MWCNTs, PPy-C, and MWCNT-doped PPy-C nanocomposite was evaluated using transmission electron microscopy (TEM) as indicated in Fig. 4. Figure 4a shows the pristine MWCNTs with an aggregated form with the nanotube diameter ranging from 5 to 10 nm. In contrast, the TEM image of Fig. 4b for the PPy-C reveals a dense irregular agglomerate morphology. This kind of agglomerated structure may obstruct the movement of electrolyte ions. Well-isolated CNT is one of the

vital factors to fabricate uniform MWCNT/PPy-C nanocomposite. Therefore, the composite preparation was carried out with a constant sonication throughout the whole process with a very dilute reaction solution. Figure 4c demonstrates that the MWCNTs were well dispersed into the PPy-C composite with disentanglement (debundling) morphology and therefore may enhance the active surface. From the HRTEM image of MWCNTs/PPy-C nanocomposite shown in Fig. 4d, one can observe that the nanotube thickness slightly increases (ca. 12–15-nm diameter) compared to pure MWCNTs, as well as their external surface is not smooth. This might happen due to the adherent ability of PPy that adsorbed onto the MWCNT sidewalls during the sonication reaction.

Electro-catalytic Performance of MWCNTs/PPy-C/GCE

The electrochemical oxidation of NO_2^- onto the as-fabricated electro-catalyst was investigated using cyclic voltammetry (CV) and electrochemical impedance spectroscopy (EIS) techniques in 0.1 M PBS electrolyte

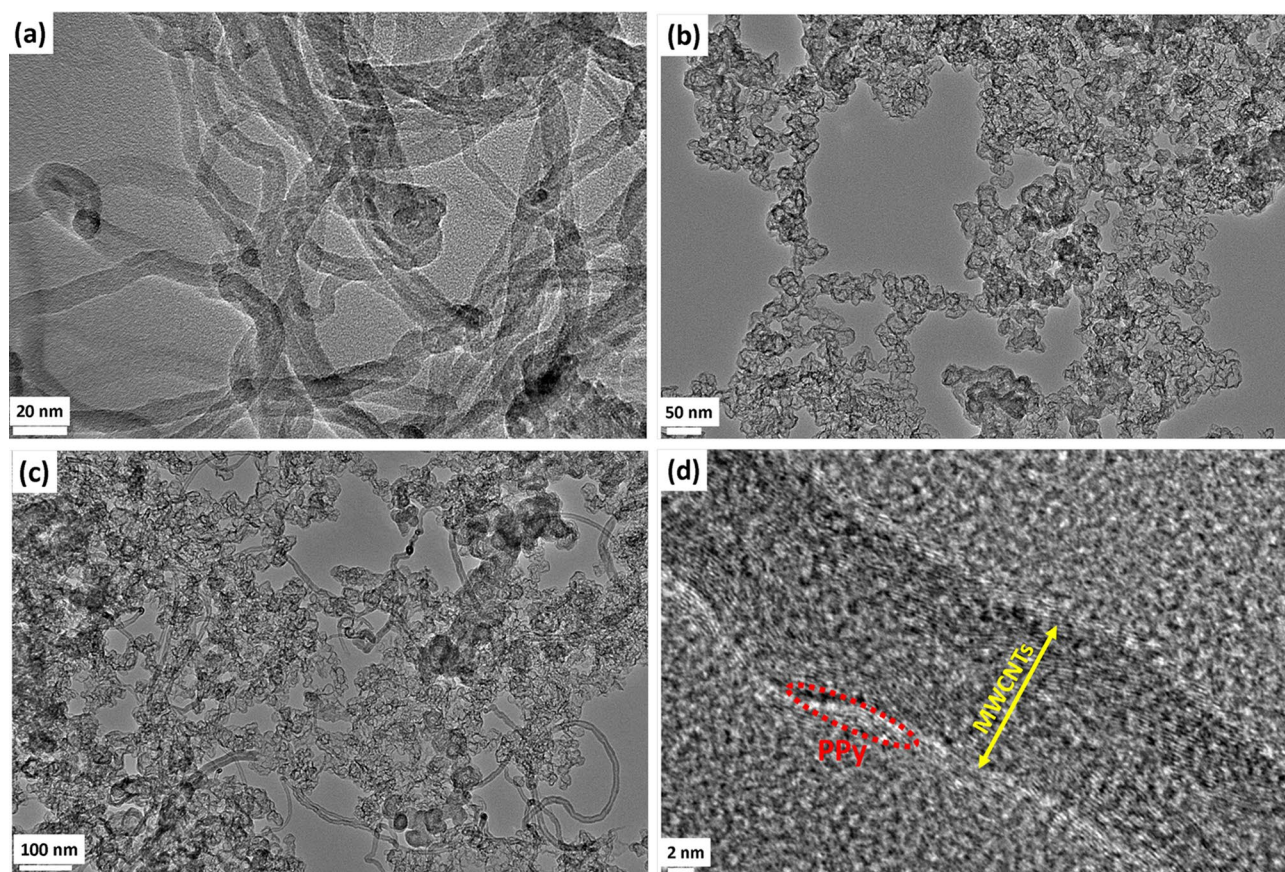


Fig. 4 TEM image (a) pristine MWCNTs, (b) PPy-C composite, (c) low-resolution, and (d) high-resolution (HRTEM) image of MWCNTs/PPy-C nanocomposite

of pH = 7.1. Figure 5a depicts the voltammograms using bare GCE, PPy-C/GCE, and MWCNTs/PPy-C/GCE in the presence of test analyte (1.0 mM NO_2^-) at a potential scan rate 25 mVs^{-1} . It was demonstrated that both GCE and PPy-C modified GCE exhibited an oxidation peak at ca. 1.25 V potential region. However, the PPy-C/GCE electrode displays a comparatively higher anodic current response compared with the unmodified GCE within the same potential region. In contrast, the MWCNTs/PPy-C/GCE electrode shows a clear peak shape with dramatically increase of oxidation current at 1.0 V potential, which is significantly lower potential (ca. 250 mV) in comparison with its counterparts. This drastic enhancement of current intensity with noticeably lowering in overpotential implies that the 5%MWCNT-doped PPy-C electro-catalyst has an outstanding sensing and catalytic performance towards NO_2^- electro-oxidation reaction. However, Fig. 5a demonstrates that MWCNTs/PPy-C/GC electrode shows higher capacitive or double-layer current included with higher oxidation current in comparison with PPy-C/GCE or unmodified GCE. The higher capacitive current might appear due to the higher surface area, which might result due to the presence of MWCNTs in fabricated nanocomposite [67]. In addition, numerous new active sites were generated due to the enlargement of catalytic surface area and this process can enhance the interaction of target analyte with as-fabricated electrocatalyst [68]. Table S1 (Supplementary Information) shows the comparison of electro-catalytic response in term of peak potential (E_p) and peak current (I_p) for nitrite electro-oxidation using different working electrodes.

To further understand the catalytic behavior of the as-fabricated catalyst towards NO_2^- electro-oxidation, the EIS investigation was carried out (Fig. 5b). The EIS is a dynamic method to measure the interfacial properties of the electro-catalyst modified electrode and can offer valuable information regarding the minor disturbance of the catalyst surface-electrolyte interfacial characteristics during the electrochemical process [69]. The EIS Nyquist plot was taken with respect to 1.0 mM NO_2^- in 0.1 M PBS under the applied potential 1.0 V, in a frequency range 10^{-2} to 10^5 Hz and a signal amplitude 10 mV. The higher electrical conductivity, e.g., the low charge transfer resistance (R_{ct}) at the surface-solution interface, was indicated when the EIS Nyquist plot showed lower semicircle diameter at a higher frequency area [70]. Herein, under the identical experimental conditions, the bare GCE shows a higher charge transfer resistance with a slow electron transfer kinetics, which indicates a lower catalytic performance. Meanwhile, both PPy-C and MWCNTs/PPy-C modified GCEs showed a lower semicircle diameter in higher frequency region, indicating higher catalytic performance towards NO_2^- electrochemical oxidation process. However, from magnifying image (Inset; Fig. 5b) of higher frequency region of EIS spectra, signposts that MWCNTs/PPy-C electrode shows the lowest semicircle diameter compared to PPy-C/GCE modified and unmodified electrodes; e.g., it showed the lowest charge transfer resistance, and higher electrical conductivity. This result reveals that MWCNT-doped PPy-C nanomaterials might facilitate the heterogeneous electron transfer process by enhancing the conductivity at the surface-solution interface and finally

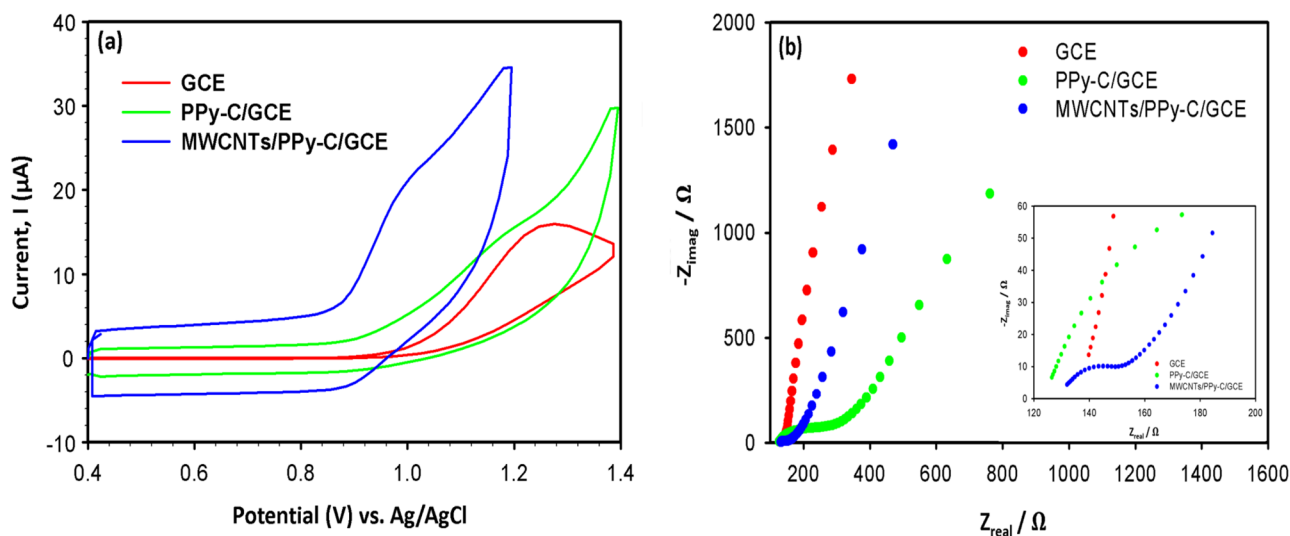


Fig. 5 (a) Cyclic voltammograms (CVs) of bare GCE, PPy-C/GCE, and MWCNTs/PPy-C/GCE in the presence of 1.0 mM NO_2^- in 0.1 M PBS (pH=7.1) at a potential scan rate 25 mVs^{-1} . (b) EIS Nyquist plot was documented in the 0.1 M PBS (pH=7.1) solution contain-

ing 1.0 mM NO_2^- of GCE, PPy-C/GCE, and MWCNTs/PPy-C/GCE; conditions: single amplitude 10 mV, applied potential 1.0 V, and the frequency range is 10^{-2} to 10^5 Hz

to facilitate the nitrite electro-oxidation process. The remarkable oxidation efficiency at lower overpotential obtained using MWCNTs/PPy-C electrocatalyst might happen due to the synergistic coupling effect. Moreover, it has been reported that MWCNTs and PPy can form a very compact structure due to the close interaction between MWCNTs and PPy [47], which might influence the synergistic coupling effect. In addition, it is also expected that MWCNTs can increase the catalytic active sites by increasing the effective surface area, and also can induce more electron transfer channels, which ultimately enhanced the catalytic performance towards nitrite ion electro-oxidation.

Kinetic Study of NO_2^- Electro-oxidation

It is mostly accepted that NO_2^- undergoes a single electron transfer oxidation reaction at various electrodes forming nitrogen dioxide (NO_2) as a product which later undergoes disproportionation reaction yielding NO_3^- as end-product [71–73]. However, to unveil the electron transfer kinetics, we recorded scan rate–dependent CVs at pH 7.1 in PBS. A steady increment of anodic current with increasing the scan rate was noticed. However, from Fig. 6a, it was observed that with increasing the scan rate, the NO_2^- oxidation peak gradually broadened as well as the peak shifted towards more positive potential direction.

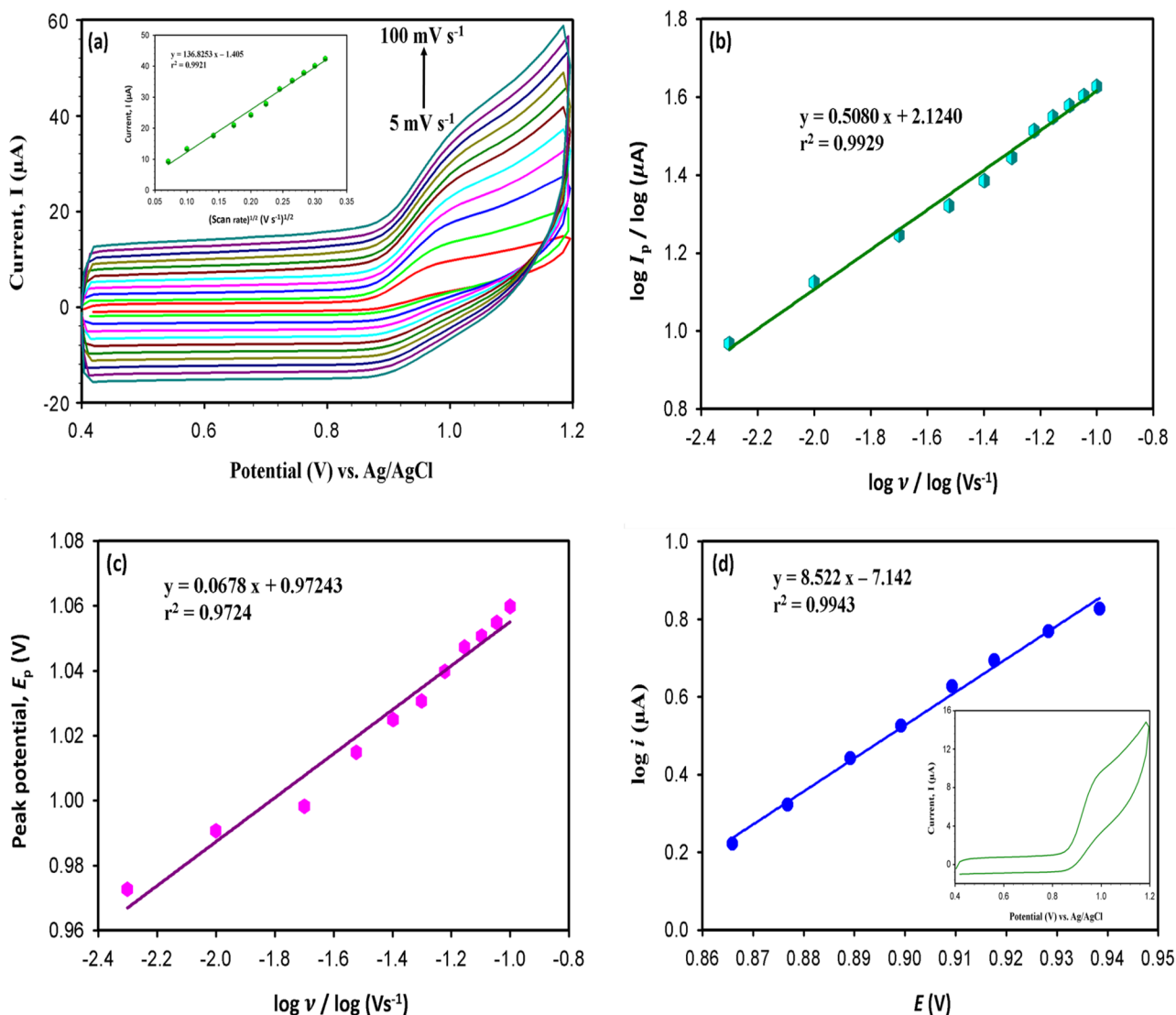


Fig. 6 (a) CV response of 1.0 mM NO_2^- in 0.1 M PBS (pH=7.1) at 5%MWCNTs/PPy-C/GCE electrode with the variation of scan rate 5 to 100 mVs^{-1} . Inset: Plot of peak current vs. sq. root of scan rate. (b) Plot of \log (peak current) vs. \log (scan rate). (c) Plot of peak

potential vs. \log (scan rate). (d) The Tafel plot resulting from the escalating part of 5 mVs^{-1} scan rate voltammogram. Inset shows the corresponding voltammogram of 5 mVs^{-1} scan rate in 1.0 mM NO_2^- concentration

The shift of peak position specifies that irreversible electrochemical process occurred in this concern oxidation reaction [18]. Furthermore, this shifting of peak position indicates the kinetic limitation of the oxidation process between the electrocatalytic active sites and the analyte (NO_2^-) [74]. Besides, a reasonable linearity was observed in Fig. 6a (inset) with the correlation co-efficient value ($r^2 = 0.99$) of the relationship of peak current (I_p) and square root of scan rate (Vs^{-1})^{1/2} with the following correlation equation: Eq. 1

$$I_p(\mu\text{A}) = 136.83v^{1/2}(\text{Vs}^{-1})^{1/2} - 1.405 \quad (1)$$

The linear relationship of peak current vs. square root of scan rate represents that the electro-oxidation process followed a diffusion controlled phenomenon [75]. Furthermore, a slope value was estimated from the linearity between log peak current ($\log I_p$ (μA)) vs. log scan rate ($\log v$ (Vs^{-1})), and the projected value was 0.508 (Fig. 6b). This result reflects that the electro-oxidation process follows a pure diffusion-controlled process. According to the literature, as theoretically for pure diffusion and adsorption process, the slope value should be 0.5 and 1.0, respectively [76, 77]. Therefore, from the above observation, it can be concluded that the NO_2^- oxidation reaction follows an irreversible diffusion-controlled process.

Tafel slope analysis plays a significant role to evaluate the electron transfer kinetics as well as electron transfer coefficient (α) value. The slope value of the peak potential (E_p (V)) vs. log scan rate ($\log v$ (Vs^{-1})) (Fig. 6c) can be used to obtain Tafel slope (b) as per the following equation [76]: Eq. 2

$$E_{p_a} = \frac{b \log v}{2} + \text{constant} \quad (2)$$

Using the slope value of E_p vs. $\log v$ and applying Eq. (2), the Tafel slope (b) value was obtained to be 135.6 mV/decade, which is higher than the regular values 30–120 mV/decade, suggesting that the NO_2^- electro-oxidation proceeds via a single electron transfer rate-determining step [74]. Then, the electron transfer co-efficient (α) between NO_2^- and MWCNTs/PPy-C/GCE electrode can be calculated using the Tafel slope (b) value according to Eq. (3) [76]

$$b = \frac{2.303RT}{(1-\alpha)n_\alpha F} \quad (3)$$

Assuming $n_\alpha = 1$, the value of α and $(1-\alpha)n_\alpha$ was projected to 0.56 and 0.44, respectively. Furthermore, the relationship between $\log i$ vs. E (Fig. 6d), commonly known as Tafel diagram can also be employed to obtain the electron transfer coefficient (α) value as well. The data

for the Tafel diagram was taken from the escalating part of the voltammogram at 5 mVs^{-1} scan rate using NO_2^- concentration 1.0 mM (Fig. 6d (inset)). The slope of linear relationship of $\log i$ vs. E ($r^2 = 0.9943$) was found to be 8.522 V^{-1} . According to the literature, this slope value corresponds to $(1-\alpha)F/2.3RT$ [78]. From this analysis, the electron transfer coefficient (α) is calculated to be 0.5. This obtained value is close to the value obtained from Eq. (3).

In this totally irreversible nitrite electro-oxidation reaction, the standard rate constant (k^0) value at ambient temperature (25°C) can be evaluated using the following equation [79]: Eq. (4)

$$k^0 = 1.11 D_0^{1/2} \left| E_p - E_{p/2} \right|^{-1/2} v^{1/2} \quad (4)$$

where E_p is the peak potential and $E_{p/2}$ is denoted as half-wave potential. By applying the above equation, at 0.05 Vs^{-1} , the value of k^0 was projected to be $5.488 \times 10^{-3} \text{ cm s}^{-1}$, representing the effective electron transfer in this concern electrochemical process.

Finally, the reaction order can be projected from the relationship of $\log i$ and $\log [\text{NO}_2^-]$. Fig. S1 shows the plot of $\log i$ vs. $\log [\text{NO}_2^-]$, which exhibits a linear relationship with the regression coefficient ($r^2 = 0.9924$) as per the following equation. The faradic currents were picked up at potential 1.0 V. Eq. (5)

$$\log i = m \log [\text{NO}_2^-] + \log k \quad (5)$$

The slope value equals to 0.846, which implies the first-order kinetics of that electro-oxidation reaction with respect to analyte (NO_2^-) concentration [80].

Voltammetric Detection of Nitrite Ions

To examine the sensing performance of the newly prepared MWCNTs/PPy-C electrocatalyst towards NO_2^- detection, LSV investigation was carried out using various concentrations of nitrite ion (0.50–10.50 mM) in 0.1 M PBS solution at a constant scan rate 10 mVs^{-1} . Figure 7a shows that the oxidation current gradually increases with the successive addition of nitrite ions into the reaction medium, signifying the sensing efficiency of as-prepared electrocatalyst. The enhancement of oxidation current with the successive injection of NO_2^- may be related to the availability of the free charges as well as the excellent charge sensing capability of the as-fabricated sensor electrode. Furthermore, a linear behavior was observed between the peak current vs. nitrite concentration with the entire concentration range (0.5–10.50 mM) of NO_2^- (Fig. 7b) with the calibration equation: Eq. (6)

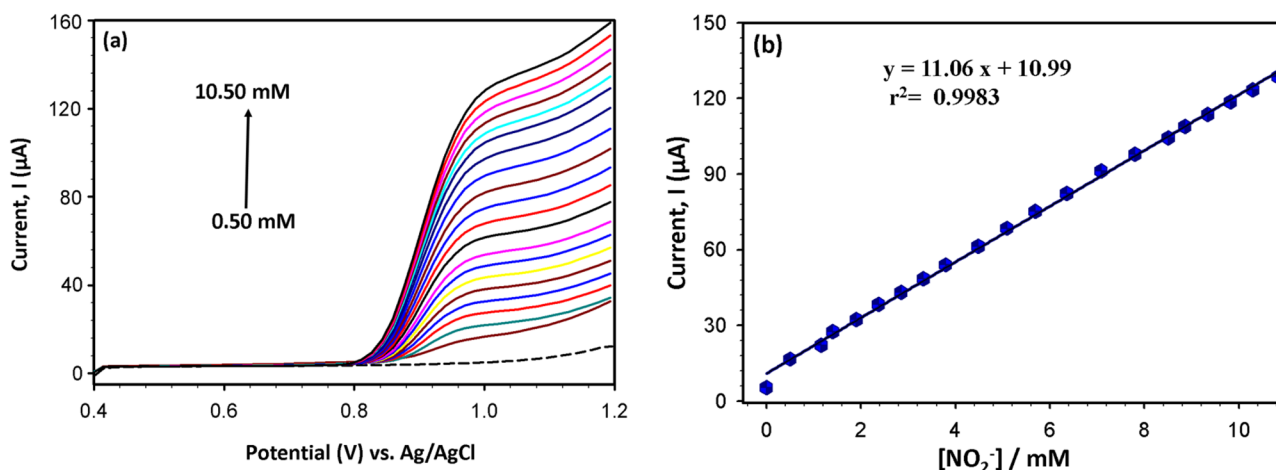


Fig. 7 (a) LSV of 5%MWCNTs/PPy-C modified GCE with respect to NO_2^- concentration in 0.1 M PBS (pH=7.1) with a scan rate 10 mVs^{-1} . The black dashed line represents a voltammogram for blank

measurement. (b) Corresponding calibration plot of peak current vs. NO_2^- concentration

please also correct format of Eq. 6 as follows: $I (\mu\text{A}) = 11.06 [\text{NO}_2^-] (\text{mM}) + 10.99 (\mu\text{A})$

$$I(\mu\text{A}) = 11.06 \frac{[\text{NO}_2^-]}{\text{mM}} + 10.99 (\mu\text{A}) \quad (6)$$

The equation fitting led to a regression coefficient $r^2 = 0.9983$ and the slope value obtained from the calibration curve is $11.06 \mu\text{AmM}^{-1}$ ($0.01106 \mu\text{A}\mu\text{M}^{-1}$). The as-fabricated sensor sensitivity was calculated by dividing the slope value with the electrode surface area (0.071 cm^2), and it was found to be $0.1558 \mu\text{A}\mu\text{M}^{-1} \text{ cm}^{-2}$. The limit of detection (LOD) was projected using Eq. (7) at a signal to noise ratio ($S/N=3$) [81]:

$$\text{LOD} = 3S_b/m \quad (7)$$

where S_b represents the standard deviation of seven measurements of blank (0.1 M PBS electrolyte without analyte), which amounted to be $0.0084868 \mu\text{A}$, and m equals to the slope of the current vs. concentration curve (Fig. 7b). From Eq. (7) the projected LOD value was calculated to be $2.30 \mu\text{M}$.

Amperometric Detection of Nitrite Ions

The sensing performance of the as-fabricated sensor electrode was further investigated by the amperometric technique. The amperometric technique can provide more sensitive and trustworthy information regarding the detection performance of the MWCNTs/PPy-C/GCE sensor compared to voltammetry techniques [82]. The amperometric technique gives a distinct current response after each addition of NO_2^- in the electrolyte medium under constant stirring at a fixed applied potential, generating a typical staircase shape. Figure 8a shows the amperometric response of

NO_2^- electro-oxidation at a constant applied potential (1.0 vs. Ag/AgCl) within the concentration range 5–9500 μM . The as-fabricated sensor electrode revealed the steady-state current response appeared after each addition of NO_2^- , with a rapid response time $<10 \text{ s}$. This result indicates that the proposed sensor electrode shows an excellent sensing performance towards NO_2^- detection. Negligible current drift was detected at lower concentration region; however, drifting was amplified at the higher concentration region. The drifting may be induced due to the potential change of reference electrode and/or change of solution pH [31]. These results reflect the stability and proper sensing activities of the as-fabricated sensor with no propensity towards surface poisoning. More details regarding the selectivity and stability will be discussed in the next section (“**Selectivity, Stability, and Reproducibility of the As-fabricated Sensor**”).

Figure 8b shows the amperometric current intensity with a linearly increased trend with the NO_2^- concentration. After linear fitting, the following regression equation (Eq. 8) was obtained: please correct format of Eq. 8 as follows: $I (\mu\text{A}) = 0.008312 [\text{NO}_2^-] (\mu\text{M}) + 2.576 (\mu\text{A})$ ($r^2 = 0.9943$)

$$I (\mu\text{A}) = 0.008312 \frac{[\text{NO}_2^-]}{\mu\text{M}} + 2.576 \mu\text{A} \quad (r^2 = 0.9943) \quad (8)$$

The sensitivity and detection limit of the as-prepared MWCNTs/PPy-C modified GC electrode was calculated to be $0.1171 \mu\text{A}\mu\text{M}^{-1} \text{ cm}^{-2}$ and $3.06 \mu\text{M}$ using the procedure utilized in the previous section (“**Voltammetric Detection of Nitrite Ions**”) for LSV case. The LOD ($3.06 \mu\text{M}$) is still lower enough than the permissible limit of NO_2^- in drinking water ($4.3 \mu\text{M}$) postulated by WHO [83]. The amperometric study was repeated using identical experimental conditions, but at 100 mV lower applied potential (0.9 V

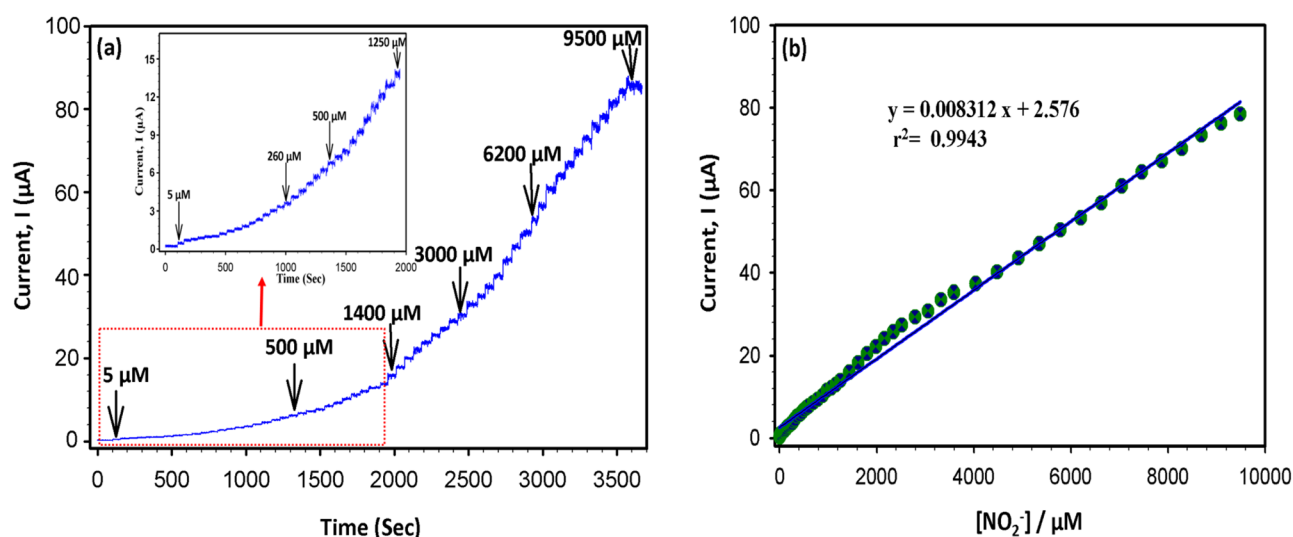


Fig. 8 (a) Amperometric (i-t) response of the 5%MWCNTs/PPy-C/GCE to the consecutive addition of NO_2^- (5–9500 μM) into a constant stirred 0.1 M PBS (pH = 7.1) solution at an applied potential 1.0 V vs. Ag/AgCl (KCl). (b) Calibration curve of current vs. analyte concentration

vs. Ag/AgCl) (Fig. S2). In this experiment, observed linear detection range was 22 to 8500 μM . By calculating the sensitivity and LOD, it was found to be $0.0386 \mu\text{A}\mu\text{M}^{-1} \text{cm}^{-2}$ and 9.43 μM , respectively. From this, the electrode sensitivity toward nitrite ion detection at potential 0.9 V is one-third compared to the sensitivity observed at 1.0 V. From the above discussion, it may conclude that 1.0 V applied potential is most suitable for NO_2^- detection in an amperometric technique using this electro-catalyst assemble. The sensing performance efficiency (in term of LOD, sensitivity, and detection range) of the current prepared MWCNTs/PPy-C/GCE sensor is quite comparable with CNTs or conductive polymer-based sensor electrode (Table 1) [8, 41, 43–45, 84–96]. The current proposed sensor exhibited a wide detection range, low detection limit, and comparable sensitivity towards NO_2^- detection. The sensitivity of the proposed sensor is better than some previously reported relevant sensor electrodes based on PANI@GO/GCE [89], MOS_2 -MWCNTs-Au [90], poly(aniline-co-o-aminophenol) (PAOA) [88], and PANI- MOS_2 [96]. By considering the LOD value, the current fabricated sensor exhibited better LOD compared to MWCNTs [41], MOS_2 -MWCNTs-Au [90], Poly(pyrrole) nanowire [92], carbon nanotube-microelectrodes (CNT-MEs) [94], silver microcubic-poly (acrylic acid)/poly (vinyl alcohol) (AgMCs-PAA/PVA) [87], and Au/ TiO_2 /CNT [85]. In general, our proposed sensor demonstrated lower detection limit compared to CNTs [41, 94] and polypyrrole [92] alone. This superb catalytic and sensing performance of the as-fabricated electro-catalyst towards NO_2^- is due to the unique catalytic properties of MWCNTs

and PPy-C nanomaterials as well as their combined synergistic effect.

Selectivity, Stability, and Reproducibility of the As-fabricated Sensor

To ensure the validity of the as-fabricated electrocatalyst for practical applications, sensor selectivity, operational stability, repeatability, and reproducibility check were conducted. The selectivity test of the MWCNTs/PPy-C modified GCE electrode was done using amperometric measurement in the existence of several metal ions and biomolecules (Fig. 9a). The interfering species, namely, KCl, CaCl_2 , Na_2SO_4 , NaNO_3 , K_2CO_3 , glucose, and oxalic acid were added separately with 5 times higher concentration than NO_2^- concentration in 0.1 M PBS solution at 1.0 V applied potential with a constant stirring. However, uric acid and dopamine were added with two times higher concentration than nitrite ion. From the amperometric current response, it was depicted as a rapid current response upon each addition of nitrite in the neutral reaction medium. Whereas excluding dopamine, all examined interfering metal ions and biomolecules have no or minimal amperometric response (Fig. 9b). However, the current modified electrode exhibited noticeable current response toward dopamine at 1.0 V applied potential. The same experiment was further conducted using LSV technique with a similar behavior obtained (Fig. S3). As revealed, except dopamine, all examined interfering ions and biomolecules have no or minimal current response at a potential near 1.0 V. These obtained results demonstrated

Table 1 A comparison of the nitrite sensing parameters (e.g., limit of detection, sensitivity, and dynamic detection range) of our proposed sensor electrode with various relevant sensor electrodes

Modified electrode	Detection method	LOD (μM)	Sensitivity ($\mu\text{A}\mu\text{M}^{-1}\text{cm}^{-2}$)	Linear range (μM)	Ref
PANI/MWCNTs/GCE	Amperometric	1.0	719.2 [#]	5–15,000	[43]
PANI@GO/GCE	Amperometric	0.5	0.117	2–44,000	[89]
PANI-MoS ₂ /GCE	Amperometric	1.5	0.02868	1034–4834	[96]
PAOA/GCE	Amperometric	2.0	0.0643	5–2000	[88]
MoS ₂ -MWCNTs-Au/GCE	Amperometric	4.0	0.001734, 0.006735	12–2100, 2100–6500	[90]
PPy/SDS/f-MWCNTs/GCE	DPV	0.11	0.017*	3–1120	[44]
PPy-Cu/GCE	Amperometric	0.03	-	0.1–1000	[91]
MWCNTs/CCE	Amperometric	35.8	-	50–3000	[41]
	DPV	4.74	-	15–220	
Rhodamine B/GCE	Amperometric	0.1	0.3081	0.5–7.0	[95]
PAA/CNTs/GCE	Amperometric	1.0	-	3–4500	[45]
Poly(Pyrrrole) nanowire/Graphite electrode	CV	228	-	228–20,000	[92]
CNTPMEs	Amperometric	8	-	16–150,000	[94]
PVN-MWNTs/CFE	Amperometric	0.05	-	0.2–3100	[8]
CS/MWCNTs/CNs/GCE	LSV	0.89	-	5–1000	[84]
AgMCs-PAA/PVA/SPCE	Amperometric	4.5	0.474	2–800	[87]
Au/TiO ₂ /CNT	DPV	3.0	-	4–225	[85]
PAR/Fe ₃ O ₄ /GCE	CV	1.19	-	9.64–1300	[86]
PEDOT/MWCNTs/SPCE		0.96	140 [#]	50–1000	[93]
MWCNTs/PPy-C/GCE	LSV	2.30	0.1558	500–10,500	Present work
MWCNTs/PPy-C/GCE	Amperometric	3.06	0.1171	5–9500	Present work

Sensitivity measured * ($\mu\text{A}\mu\text{M}^{-1}$), [#] $\text{mA}^{-1}\text{M}^{-1}\text{cm}^{-2}$

PAOA poly(aniline-co-o-aminophenol), CCE carbon ceramic electrode, CNTPMEs carbon nanotubes powder microelectrodes, CFE carbon fiber electrode, CS chitosan, CNs carbon nanoparticles, AgMCs-PAA/PVA/SPCE silver microcubics-poly (acrylic acid)/poly (vinyl alcohol)/screen printed microelectrode, PAR poly-(Alizarin Red)

the excellent selective behavior of the as-fabricated CNTs/PPy-C nanocomposite towards nitrite ion electro-oxidation.

The operational stability of the newly fabricated catalyst modified GC electrode towards nitrite electro-oxidation was

performed by a continuous 75-min amperometric measurement (Fig. S4). It was found that after 75 min, ca. 90% of the initial current intensity was retained. This result reflects the excellent operational stability of the proposed sensor

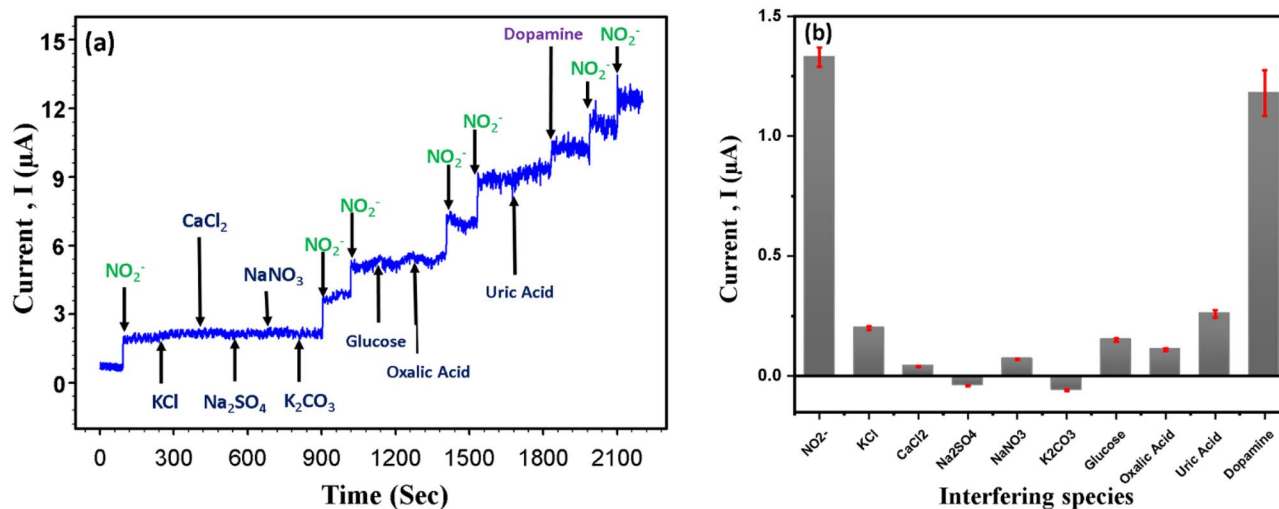


Fig. 9 (a) The selectivity test of MWCNTs/C-PPy modified GCE upon the addition of $100\ \mu\text{M}\ \text{NO}_2^-$ and $500\ \mu\text{M}$ interfering species, namely, KCl, CaCl_2 , Na_2SO_4 , NaNO_3 , K_2CO_3 , glucose, and oxalic

acid and $200\ \mu\text{M}$ uric acid and dopamine in $0.1\ \text{M}$ PBS ($\text{pH}=7.1$) at $1.0\ \text{V}$ applied potential. (b) The current response with error bar in presence of interfering species

for NO_2^- detection in the neutral medium. In addition, the repeatability of the fabricated electrode was investigated using CV with 25 repeated cycles (Fig. S5). The result reveals that after 25 cycles, the current intensity was retained ca. 89% from its initial value with % RSD 4.60. This result is consistent with the amperometric measurement. Moreover, the reproducibility of the as-fabricated electrocatalyst was examined via fabricating three different GC electrodes modified with the same modification conditions (Fig. S6). Thereafter, the CV experiment was conducted at identical experimental conditions; the anodic current at these three electrodes shows a minor fluctuation with a relative standard deviation (% RSD) 5.00%, indicating acceptable reproducibility of the as-fabricated sensor electrode.

From the above discussion, it is concluded that the newly prepared electrocatalyst shows good selectivity towards NO_2^- in amperometric detection even in the existence of several common interfering metal ions and biomolecules. In case of dopamine, the dopamine shows sensitivity in this applied potential range; however, even after dopamine presence, the sensor electrode retained its sensitivity towards nitrite ion detection. Moreover, the operational stability and reproducibility results suggest that the newly prepared electro-catalyst could serve as a trustworthy platform for the detection of NO_2^- as an electrochemical sensor.

Real Sample Analysis

To confirm the validity of the as-fabricated sensor in real-life application, we have employed amperometric study to check the practical aptness of MWCNTs/PPy-C modified sensor for the recovery of NO_2^- from tap water and deep-well water applying the standard addition method. Three different concentrations of NO_2^- was injected into the tap water sample in 0.1 M PBS, and the current response was recorded at 1.0 V applied potential. The measurement was conducted three times for each sample and found the acceptable recovery with %RSD 2.12 to 3.26 (Table S2). In addition, the deep-well water was collected from Najran Velly, Jurbah, Najran, Saudi Arabia. The measurement was also conducted three times for each sample using the standard addition method with an acceptable recovery of % RSD 1.60 to 3.22 (Table S3). These results indicate that the current fabricated nanocomposite is an anticipating electro-catalyst for the efficient detection of NO_2^- from real samples.

Conclusions

In summary, a simple sonochemical technique was employed to synthesize a novel MWCNTs/PPy-C nanocomposite. Then, drop-casting technique was used to fabricate the nanocomposite modified GCE and subsequently applied for the

electrocatalytic oxidation and detection of NO_2^- . The close interaction between MWCNTs and PPy produced a compact structure with a high active surface area. It was observed that the as-fabricated nanocomposite shows higher catalytic efficiency than the bare GCE or the PPy-C composite modified GCE. This is probably due to a synergistic coupling effect between the base materials as well as a significant enrichment of catalytic active sites due to the incorporation of MWCNTs into the PPy-C composite. The kinetic analytical results revealed that the nitrite ion oxidation reaction follows the first order diffusion-controlled kinetics process. By evaluating Tafel slope, it was estimated that this oxidation reaction involves a single electron transfer at the rate determining step, where NO_2 is the intermediate, which can later undergo disproportionation reaction yielding NO_3^- as end product. The electron transfer co-efficient (α) was estimated to be 0.56 from E_p vs. $\log \nu$ relationship and 0.5 from the Tafel diagram ($\log i$ vs. E). From LSV study, the as-fabricated sensor shows a sensitivity of $0.1558 \mu\text{A}\mu\text{M}^{-1} \text{cm}^{-2}$ in a dynamic concentration range 0.50–10.50 mM, whereas the amperometric result revealed a sensitivity of $0.1171 \mu\text{A}\mu\text{M}^{-1} \text{cm}^{-2}$ over the nitrite concentration range 5–9500 μM . In NO_2^- detection, the as-fabricated sensor exhibited excellent stability, repeatability, reproducibility, and considerable selectivity during the interference study in the existence of several common metal ions and biomolecules. Furthermore, this fabricated sensor electrode was effectively investigated for the recovery of NO_2^- from tap water and deep-well water samples as real sample analysis. The findings revealed that the combination of carbon nanomaterial and organic conductive polymer might be a promising candidate for the efficient electrochemical sensor applications.

Supplementary Information The online version contains supplementary material available at <https://doi.org/10.1007/s12678-021-00675-6>.

Acknowledgements The authors are thankful to the Deanship of Scientific Research at Najran University, Kingdom of Saudi Arabia for funding this work through a Grant: Research code NU/ESCI/17/019.

Author Contribution Md. A. Rashed: methodology, investigation, formal analysis, original draft preparation; M. Faisal: formal analysis, validation, writing—review and editing; Mabkhoot Alsaari: data curation, writing—review and editing; S.A. Alsareii: validation, resources, writing—review and editing; Farid A. Harraz: conceptualization, writing—review and editing, visualization, supervision. All the authors revised and approved the manuscript.

Funding The authors received financial support from the Deanship of Scientific Research at Najran University, Kingdom of Saudi Arabia, through a Grant: Research code NU/ESCI/17/019. Md. Abu Rashed also received support from the Research and Development Office, the Deputyship for Research & Innovation, Ministry of Education, Kingdom of Saudi Arabia, in cooperation with Najran University in the form of a post-doctoral fellowship.

Declarations

Conflict of Interest The authors declare no competing interests.

References

1. C. Menard, F. Heraud, J.L. Volatier, J.C. Leblanc, Assessment of dietary exposure of nitrate and nitrite in France. *Food Addit. Contam. – Part A Chem. Anal. Control. Expo. Risk Assess* **25**, 971–988 (2008). <https://doi.org/10.1080/02652030801946561>
2. M.A. El-Asasery, Solvent-free one-pot synthesis of some azo disperse dyes under microwave irradiation: Dyeing of polyester fabrics. *J. Appl. Polym. Sci* **109**, 695–699 (2008). <https://doi.org/10.1002/app.28129>
3. S. Hosoya, Sulfuric acid bleaching of kraft pulp II: Behavior of lignin and carbohydrate during sulfuric acid bleaching. *J. Wood Sci* **45**, 313–318 (1999). <https://doi.org/10.1007/bf00833496>
4. J.S. Reou, K.Y. Ann, The electrochemical assessment of corrosion inhibition effect of calcium nitrite in blended concretes. *Mater. Chem. Phys* **109**, 526–533 (2008). <https://doi.org/10.1016/j.matchemphys.2007.12.030>
5. W.J.R. Santos, P.R. Lima, A.A. Tanaka, S.M.C.N. Tanaka, L.T. Kubota, Determination of nitrite in food samples by anodic voltammetry using a modified electrode. *Food Chem* **113**, 1206–1211 (2009). <https://doi.org/10.1016/j.foodchem.2008.08.009>
6. P.F. Swann, The toxicology of nitrate, nitrite and n-nitroso compounds. *J. Sci. Food Agric* **26**, 1761–1770 (1975). <https://doi.org/10.1002/jsfa.2740261119>
7. A. Amine, G. Palleschi, phosphate, nitrate, and sulfate biosensors. *Anal. Lett.* **37**, 1–19 (2004). <https://doi.org/10.1081/AL-120027770>
8. D. Zheng, C. Hu, Y. Peng, S. Hu, A carbon nanotube/polyvanillin composite film as an electrocatalyst for the electrochemical oxidation of nitrite and its application as a nitrite sensor. *Electrochim. Acta.* **54**, 4910–4915 (2009). <https://doi.org/10.1016/j.electacta.2009.04.004>
9. M.A. Hasnat, M.A. Rashed, M.S. Alam, M.M. Rahman, M.A. Islam, S. Hossain, N. Ahmed, Electrocatalytic reduction of NO₂⁻: platinum modified glassy carbon electrode. *Catal. Commun.* **11**, 1085–1089 (2010). <https://doi.org/10.1016/j.catcom.2010.05.015>
10. T.Y.K. Chan, Vegetable-borne nitrate and nitrite and the risk of methaemoglobinaemia. *Toxicol. Lett.* **200**, 107–108 (2011). <https://doi.org/10.1016/j.toxlet.2010.11.002>
11. H. Xu, J. Peng, M. Zhu, J. Liu, Ultrasensitive detection of nitrite based on gold-nanoparticles/polyrhodamine B/carbon nanotubes modified glassy carbon electrode with enhanced electrochemical performance. *Int. J. Electrochem. Sci.* **12**, 10642–10659 (2017). <https://doi.org/10.20964/2017.11.48>
12. W. Frenzel, J. Schulz-Brüssel, B. Zinvirt, Characterisation of a gas-diffusion membrane-based optical flow-through sensor exemplified by the determination of nitrite *Talanta.* **64**(278), 282 (2004). <https://doi.org/10.1016/j.talanta.2004.01.025>
13. K. Zhang, Y. Hu, G. Li, Diazotization-coupling reaction-based selective determination of nitrite in complex samples using shell-isolated nanoparticle-enhanced Raman spectroscopy. *Talanta* **116**, 712–718 (2013). <https://doi.org/10.1016/j.talanta.2013.07.019>
14. E. Pagliano, J. Meija, Z. Mester, High-precision quadruple isotope dilution method for simultaneous determination of nitrite and nitrate in seawater by GCMS after derivatization with triethylxonium tetrafluoroborate. *Anal. Chim. Acta.* **824**, 36–41 (2014). <https://doi.org/10.1016/j.aca.2014.03.018>
15. H. Wang, F. Wen, Y. Chen, T. Sun, Y. Meng, Y. Zhang, Electrocatalytic determination of nitrite based on straw cellulose/molybdenum sulfide nanocomposite. *Biosens. Bioelectron.* **85**, 692–697 (2016). <https://doi.org/10.1016/j.bios.2016.05.078>
16. B. Strehlitz, B. Gründig, W. Schumacher, P.M.H. Kroneck, K.-D. Vorlop, H. Kotte, A nitrite sensor based on a highly sensitive nitrite reductase mediator-coupled amperometric detection. *Anal. Chem.* **68**, 807–816 (1996). <https://doi.org/10.1021/ac950692n>
17. M.A. Rashed, M. Faisal, F.A. Harraz, M. Jalalah, M. Alsaiani, M.S. Al-Assiri, rGO/ZnO/Nafion nanocomposite as highly sensitive and selective amperometric sensor for detecting nitrite ions (NO₂⁻). *J. Taiwan Inst. Chem. Eng.* **112**, 345–356 (2020). <https://doi.org/10.1016/j.jtice.2020.05.015>
18. C.A. Caro, F. Bedioui, J.H. Zagal, Electrocatalytic oxidation of nitrite on a vitreous carbon electrode modified with cobalt phthalocyanine. *Electrochim. Acta.* **47**, 1489–1494 (2002). [https://doi.org/10.1016/S0013-4686\(01\)00875-1](https://doi.org/10.1016/S0013-4686(01)00875-1)
19. W.S. Cardoso, Y. Gushikem, Electrocatalytic oxidation of nitrite on a carbon paste electrode modified with Co(II) porphyrin adsorbed on SiO₂/SnO₂/Phosphate prepared by the sol–gel method. *J. Electroanal. Chem.* **583**, 300–306 (2005). <https://doi.org/10.1016/j.jelechem.2005.06.015>
20. J.A. Wargon, A.J. Arvia, Kinetics and mechanism of the electrochemical oxidation of nitrite ion dissolved as sodium nitrite in dimethylsulphoxide solutions on platinum electrodes. *Electrochim. Acta.* **17**, 649–664 (1972). [https://doi.org/10.1016/0013-4686\(72\)80066-5](https://doi.org/10.1016/0013-4686(72)80066-5)
21. Y. Li, S. Wu, Y. Chen, Q. Lu, L. Wang, Formation of Au nano-flowers on cysteamine monolayer and their electrocatalytic oxidation of nitrite. *Anal. Methods.* **3**, 1399–1404 (2011). <https://doi.org/10.1039/c1ay05062a>
22. S.Y. Ha, S. Kim, Preparation and characterization of sol–gel derived carbon composite ceramic electrodes: electrochemical and XANES study of nitrite reduction. *J. Electroanal. Chem.* **468**, 131–138 (1999). [https://doi.org/10.1016/S0022-0728\(99\)00152-7](https://doi.org/10.1016/S0022-0728(99)00152-7)
23. H. Liu, P. He, Z. Li, C. Sun, L. Shi, Y. Liu, G. Zhu, J. Li, An ionic liquid-type carbon paste electrode and its polyoxometalate-modified properties. *Electrochem. Commun.* **7**, 1357–1363 (2005). <https://doi.org/10.1016/j.elecom.2005.09.018>
24. H. Xian, P. Wang, Y. Zhou, Q. Lu, S. Wu, Y. Li, L. Wang, Electrochemical determination of nitrite via covalent immobilization of a single-walled carbon nanotubes and single stranded deoxy-ribonucleic acid nanocomposite on a glassy carbon electrode. *Microchim. Acta.* **171**, 63–69 (2010). <https://doi.org/10.1007/s00604-010-0404-3>
25. B.R. Kozub, N.V. Rees, R.G. Compton, Electrochemical determination of nitrite at a bare glassy carbon electrode; why chemically modify electrodes? *Sensors Actuators B Chem.* **143**, 539–546 (2010). <https://doi.org/10.1016/j.snb.2009.09.065>
26. F.H. Narouei, H.K. Tammandani, Y. Ghalandarzahi, N. Sabbaghi, M. Noroozifar, An electrochemical sensor based on conductive polymers/graphite paste electrode for simultaneous determination of dopamine, uric acid and tryptophan in biological samples. *Int. J. Electrochem. Sci.* **12**, 7739–7753 (2017). <https://doi.org/10.20964/2017.08.50>
27. Z. Zhang, S. Zhai, M. Wang, L. He, D. Peng, S. Liu, Y. Yang, S. Fang, H. Zhang, Electrochemical sensor based on a polyaniline-modified SnO₂ nanocomposite for detecting ethephon. *Anal. Methods.* **7**, 4725–4733 (2015). <https://doi.org/10.1039/C5AY01028D>
28. S.M. Oliveira, J.M. Luzardo, L.A. Silva, D.C. Aguiar, C.A. Senna, R. Verdán, A. Kuznetsov, T.L. Vasconcelos, B.S. Archanjo, C.A. Achete, E. D’Elia, J.R. Araujo, High-performance electrochemical sensor based on molecularly imprinted polypyrrole-graphene modified glassy carbon electrode. *Thin Solid Films* **699**, (2020) <https://doi.org/10.1016/j.tsf.2020.137875>
29. J. Rubio Retama, E. López Cabarcos, D. Mecerreyes, B. López-Ruiz, Design of an amperometric biosensor using polypyrrole-microgel

- composites containing glucose oxidase. *Biosens. Bioelectron.* **20**, 1111–1117 (2004). <https://doi.org/10.1016/j.bios.2004.05.018>
30. M. Afshari, M. Dinari, M.M. Momeni, The graphitic carbon nitride/polyaniline/silver nanocomposites as a potential electrocatalyst for hydrazine detection. *J. Electroanal. Chem.* **833**, 9–16 (2019). <https://doi.org/10.1016/j.jelechem.2018.11.022>
 31. F.A. Harraz, A.A. Ismail, S.A. Al-Sayari, A. Al-Hajry, M.S. Al-Assiri, Highly sensitive amperometric hydrazine sensor based on novel α -Fe₂O₃/crosslinked polyaniline nanocomposite modified glassy carbon electrode. *Sensors Actuators B Chem.* **234**, 573–582 (2016). <https://doi.org/10.1016/j.snb.2016.05.021>
 32. M. Faisal, F.A. Harraz, A.E. Al-Salami, S.A. Al-Sayari, A. Al-Hajry, M.S. Al-Assiri, Polythiophene/ZnO nanocomposite-modified glassy carbon electrode as efficient electrochemical hydrazine sensor. *Mater. Chem. Phys.* **214**, 126–134 (2018). <https://doi.org/10.1016/j.matchemphys.2018.04.085>
 33. M. Faisal, M.A. Rashed, M.M. Abdullah, F.A. Harraz, M. Jalalah, M.S. Al-Assiri, Efficient hydrazine electrochemical sensor based on PANI doped mesoporous SrTiO₃ nanocomposite modified glassy carbon electrode. *J. Electroanal. Chem.* **879**, 114805 (2020). <https://doi.org/10.1016/j.jelechem.2020.114805>
 34. A. Bhattacharya, A. De, Conducting composites of polypyrrole and polyaniline a review. *Prog. Solid State Chem.* **24**, 141–181 (1996). [https://doi.org/10.1016/0079-6786\(96\)00002-7](https://doi.org/10.1016/0079-6786(96)00002-7)
 35. L.-X. Wang, X.-G. Li, Y.-L. Yang, Preparation, properties and applications of polypyrroles. *React. Funct. Polym.* **47**, 125–139 (2001). [https://doi.org/10.1016/S1381-5148\(00\)00079-1](https://doi.org/10.1016/S1381-5148(00)00079-1)
 36. B. O'Regan, M. Grätzel, © 199 1 Nature Publishing Group □ 라첼 매. *Nature* **354**, 737–740 (1991)
 37. L. Agüí, P. Yáñez-Sedeño, J.M. Pingarrón, Role of carbon nanotubes in electroanalytical chemistry: a review. *Anal. Chim. Acta.* **622**, 11–47 (2008). <https://doi.org/10.1016/j.aca.2008.05.070>
 38. D. Wang, B. Huang, J. Liu, X. Guo, G. Abudukeyoumu, Y. Zhang, B.-C. Ye, Y. Li, A novel electrochemical sensor based on Cu@Ni/MWCNTs nanocomposite for simultaneous determination of guanine and adenine. *Biosens. Bioelectron.* **102**, 389–395 (2018). <https://doi.org/10.1016/j.bios.2017.11.051>
 39. T.M.B.F. Oliveira, S. Morais, New generation of electrochemical sensors based on multi-walled carbon nanotubes. *Appl. Sci.* **8**, 5–7 (2018). <https://doi.org/10.3390/app8101925>
 40. E. Lahiff, C. Lynam, N. Gilmartin, R. O'Kennedy, D. Diamond, The increasing importance of carbon nanotubes and nanostructured conducting polymers in biosensors. *Anal. Bioanal. Chem.* **398**, 1575–1589 (2010). <https://doi.org/10.1007/s00216-010-4054-4>
 41. M.R. Majidi, A. Naseri, S. Panahian, R.F.B. Baj, Electrocatalytic oxidation and determination of nitrite at multi-walled carbon nanotubes modified carbon ceramic electrode. *J. Chinese Chem. Soc.* **60**, 314–320 (2013). <https://doi.org/10.1002/jccs.201200365>
 42. L. Zhang, W. Du, A. Nautiyal, Z. Liu, X. Zhang, Recent progress on nanostructured conducting polymers and composites: synthesis, application and future aspects. *Sci. China Mater.* **61**, 303–352 (2018). <https://doi.org/10.1007/s40843-017-9206-4>
 43. M. Guo, J. Chen, J. Li, B. Tao, S. Yao, Fabrication of polyaniline/carbon nanotube composite modified electrode and its electrocatalytic property to the reduction of nitrite. *Anal. Chim. Acta.* **532**, 71–77 (2005). <https://doi.org/10.1016/j.aca.2004.10.045>
 44. A.D. Arulraj, E. Sundaram, V.S. Vasantha, B. Neppolian, Polypyrrole with a functionalized multi-walled carbon nanotube hybrid nanocomposite: a new and efficient nitrite sensor. *New J. Chem.* **42**, 3748–3757 (2018). <https://doi.org/10.1039/c7nj04130f>
 45. J. Zeng, W. Wei, X. Zhai, P. Yang, J. Yin, L. Wu, X. Liu, K. Liu, S. Gong, Assemble-electrodeposited ultrathin conducting poly(azure A) at a carbon nanotube-modified glassy carbon electrode, and its electrocatalytic properties to the reduction of nitrite. *Microchim. Acta.* **155**, 379–386 (2006). <https://doi.org/10.1007/s00604-006-0570-5>
 46. L. Jiang, R. Wang, X. Li, L. Jiang, G. Lu, Electrochemical oxidation behavior of nitrite on a chitosan-carboxylated multiwalled carbon nanotube modified electrode. *Electrochem. Commun.* **7**, 597–601 (2005). <https://doi.org/10.1016/j.elecom.2005.04.009>
 47. P. Gemeiner, J. Kuliček, M. Mikula, M. Hatala, L. Švorc, L. Hlavatá, M. Mičušík, M. Omastová, Polypyrrole-coated multiwalled carbon nanotubes for the simple preparation of counter electrodes in dye-sensitized solar cells. *Synth. Met.* **210**, 323–331 (2015). <https://doi.org/10.1016/j.synthmet.2015.10.020>
 48. A.J. Haider, M.R. Mohammed, D.S. Ahmed, Preparation and characterization of multi walled carbon nanotubes/Ag nanoparticles hybrid materials. *Int. J. Sci. Eng. Res.* **5**, 255–261 (2014)
 49. I.Y. Jeon, H.J. Choi, L.S. Tan, J.B. Baek, Nanocomposite prepared from in situ grafting of polypyrrole to aminobenzoyl-functionalized multiwalled carbon nanotube and its electrochemical properties. *J. Polym. Sci. Part A Polym. Chem.* **49**, 2529–2537 (2011). <https://doi.org/10.1002/pola.24684>
 50. A. Dobrzańska-Danikiewicz, D. Łukowiec, J. Kubacki, Investigations of electron properties of carbon nanotubes decorated with platinum nanoparticles with their varying fraction. *J. Nanomater.* **2016** (2016). <https://doi.org/10.1155/2016/4942398>
 51. M. Li, M. Boggs, T.P. Beebe, C.P. Huang, Oxidation of single-walled carbon nanotubes in dilute aqueous solutions by ozone as affected by ultrasound. *Carbon N. Y.* **46**, 466–475 (2008). <https://doi.org/10.1016/j.carbon.2007.12.012>
 52. H. Wang, A. Zhou, F. Peng, H. Yu, J. Yang, Mechanism study on adsorption of acidified multiwalled carbon nanotubes to Pb(II). *J. Colloid Interface Sci.* **316**, 277–283 (2007). <https://doi.org/10.1016/j.jcis.2007.07.075>
 53. M. Kusunoki, H. Kato, High-density and well-aligned carbon nanotubes formed by surface decomposition of SiC. *Appl. Surf. Sci.* **254**, 257–261 (2007). <https://doi.org/10.1016/j.apsusc.2007.07.106>
 54. L. Ruangchuay, J. Schwank, A. Sirivat, Surface degradation of α -naphthalene sulfonate-doped polypyrrole during XPS characterization. *Appl. Surf. Sci.* **199**, 128–137 (2002). [https://doi.org/10.1016/S0169-4332\(02\)00564-0](https://doi.org/10.1016/S0169-4332(02)00564-0)
 55. N. Su, H.B. Li, S.J. Yuan, S.P. Yi, E.Q. Yin, Synthesis and characterization of polypyrrole doped with anionic spherical polyelectrolyte brushes. *Express Polym. Lett.* **6**, 697–705 (2012). <https://doi.org/10.3144/expresspolymlett.2012.75>
 56. K.A. Wepasnick, B.A. Smith, J.L. Bitter, D. Howard Fairbrother, Chemical and structural characterization of carbon nanotube surfaces. *Anal. Bioanal. Chem.* **396**, 1003–1014 (2010). <https://doi.org/10.1007/s00216-009-3332-5>
 57. H. Ge, G. Qi, E.-T. Kang, K.G. Neoh, Study of overoxidized polypyrrole using X-ray photoelectron spectroscopy. *Polymer (Guildf)*. **35**, 504–508 (1994). [https://doi.org/10.1016/0032-3861\(94\)90503-7](https://doi.org/10.1016/0032-3861(94)90503-7)
 58. J. Tabačiarová, M. Mičušík, P. Fedorko, M. Omastová, Study of polypyrrole aging by XPS, FTIR and conductivity measurements. *Polym. Degrad. Stab.* **120**, 392–401 (2015). <https://doi.org/10.1016/j.polymdegradstab.2015.07.021>
 59. J. Fan, M. Wan, D. Zhu, B. Chang, Z. Pan, S. Xie, Synthesis, characterizations, and physical properties of carbon nanotubes coated by conducting polypyrrole. *J. Appl. Polym. Sci.* **74**, 2605–2610 (1999). [https://doi.org/10.1002/\(SICI\)1097-4628\(19991209\)74:11%3c2605::AID-APP6%3e3.0.CO;2-R](https://doi.org/10.1002/(SICI)1097-4628(19991209)74:11%3c2605::AID-APP6%3e3.0.CO;2-R)
 60. A.C. Ferrari, Raman spectroscopy of graphene and graphite: disorder, electron–phonon coupling, doping and nonadiabatic effects. *Solid State Commun.* **143**, 47–57 (2007). <https://doi.org/10.1016/j.ssc.2007.03.052>
 61. M. Jinno, Y. Ando, S. Bandow, J. Fan, M. Yudasaka, S. Iijima, Raman scattering study for heat-treated carbon nanotubes: the origin of $\approx 1855\text{cm}^{-1}$ Raman band. *Chem. Phys. Lett.* **418**, 109–114 (2006). <https://doi.org/10.1016/j.cplett.2005.10.089>

62. X. Zhao, Y. Ando, Y. Liu, M. Jinno, T. Suzuki, Carbon nanowire made of a long linear carbon chain inserted inside a multiwalled carbon nanotube. *Phys. Rev. Lett.* **90**, 187401 (2003). <https://doi.org/10.1103/PhysRevLett.90.187401>
63. B. Zhang, Y. Xu, Y. Zheng, L. Dai, M. Zhang, J. Yang, Y. Chen, X. Chen, J. Zhou, A facile synthesis of polypyrrole/carbon nanotube composites with ultrathin, uniform and thickness-tunable polypyrrole shells. *Nanoscale Res. Lett.* **6**, 1–9 (2011). <https://doi.org/10.1186/1556-276X-6-431>
64. B.P. Singh, V. Choudhary, S. Teotia, T.K. Gupta, V.N. Singh, S.R. Dhakate, R.B. Mathur, Solvent free, efficient, industrially viable, fast dispersion process based amine modified MWCNT reinforced epoxy composites of superior mechanical properties. *Adv. Mater. Lett.* **6**, 104–113 (2015). <https://doi.org/10.5185/amlett.2015.5612>
65. M. Raja, A.M. Shanmugharaj, S.H. Ryu, Influence of surface functionalized carbon nanotubes on the properties of polyurethane nanocomposites. *Soft Mater.* **6**, 65–74 (2008). <https://doi.org/10.1080/15394450802046895>
66. H. Guo, H. Zhu, H. Lin, J. Zhang, Polypyrrole-multi-walled carbon nanotube nanocomposites synthesized in oil-water micro-emulsion. *Colloid Polym. Sci.* **286**, 587–591 (2008). <https://doi.org/10.1007/s00396-007-1828-0>
67. G. Eom, C. Oh, J. Moon, H. Kim, M.K. Kim, K. Kim, J.W. Seo, T. Kang, H.J. Lee, Highly sensitive and selective detection of dopamine using overoxidized polypyrrole/sodium dodecyl sulfate-modified carbon nanotube electrodes. *J. Electroanal. Chem.* **848**, 113295 (2019). <https://doi.org/10.1016/j.jelechem.2019.113295>
68. H. Song, X. Zhang, Y. Liu, Z. Su, Developing graphene-based nanohybrids for electrochemical sensing. *Chem. Rec.* **19**, 534–549 (2019). <https://doi.org/10.1002/tcr.201800084>
69. published by Dove Press, IJN-152163-a-hydrogel-biosensor-for-high-selective-and-sensitive-detect, (2018) 843–856. <https://doi.org/10.2147/IJN.S152163>
70. J. Hao, L. Ji, K. Wu, N. Yang, Electrochemistry of ZnO@reduced graphene oxides. *Carbon N. Y.* **130**, 480–486 (2018). <https://doi.org/10.1016/j.carbon.2018.01.018>
71. R. Guidelli, F. Pergola, G. Raspi, Voltammetric behavior of nitrite ion on platinum in neutral and weakly acidic media. *Anal. Chem.* **44**, 745–755 (1972). <https://doi.org/10.1021/ac60312a018>
72. A. Afkhami, F. Soltani-Felehgari, T. Madrakian, H. Ghaedi, Surface decoration of multi-walled carbon nanotubes modified carbon paste electrode with gold nanoparticles for electro-oxidation and sensitive determination of nitrite. *Biosens. Bioelectron.* **51**, 379–385 (2014). <https://doi.org/10.1016/j.bios.2013.07.056>
73. M.S. Alam, M.F. Shabik, M.M. Rahman, M. del Valle, M.A. Hasnat, Enhanced electrocatalytic effects of Pd particles immobilized on GC surface on the nitrite oxidation reactions. *J. Electroanal. Chem.* **839**, 1–8 (2019). <https://doi.org/10.1016/j.jelechem.2019.02.058>
74. M.A. Kamyabi, F. Aghajanloo, Electrocatalytic oxidation and determination of nitrite on carbon paste electrode modified with oxovanadium(IV)-4-methyl salophen. *J. Electroanal. Chem.* **614**, 157–165 (2008). <https://doi.org/10.1016/j.jelechem.2007.11.026>
75. C.K. Nguyen, N.Q. Tran, T.P. Nguyen, D.H. Nguyen, Biocompatible nanomaterials based on dendrimers, hydrogels and hydrogel nanocomposites for use in biomedicine. *Adv. Nat. Sci. Nanosci. Nanotechnol.* **8**, (2017). <https://doi.org/10.1088/2043-6254/8/1/015001>
76. N. Jaiswal, I. Tiwari, C.W. Foster, C.E. Banks, Highly sensitive amperometric sensing of nitrite utilizing bulk-modified MnO₂ decorated Graphene oxide nanocomposite screen-printed electrodes. *Electrochim. Acta.* **217**, 255–266 (2017). <https://doi.org/10.1016/j.electacta.2017.01.007>
77. R. Gupta, S.K. Guin, S.K. Aggarwal, A mechanistic study on the electrocatalysis of the Pu(IV)/Pu(III) redox reaction at a platinum electrode modified with single-walled carbon nanotubes (SWCNTs) and polyaniline (PANI). *RSC Adv.* **2**, 1810–1819 (2012). <https://doi.org/10.1039/c1ra01010g>
78. H.M. Nassef, A.-E. Radi, C.K. O'Sullivan, Electrocatalytic oxidation of hydrazine at o-aminophenol grafted modified glassy carbon electrode: Reusable hydrazine amperometric sensor. *J. Electroanal. Chem.* **592**, 139–146 (2006). <https://doi.org/10.1016/j.jelechem.2006.05.007>
79. J. González Velasco, Determination of standard rate constants for electrochemical irreversible processes from linear sweep voltammograms. *Electroanalysis.* **9**, 880–882 (1997). <https://doi.org/10.1002/elan.1140091116>
80. M.A. Hasnat, S. Ben Aoun, S.M. Nizam Uddin, M.M. Alam, P.P. Koay, S. Amertharaj, M.A. Rashed, M.M. Rahman, N. Mohamed, Copper-immobilized platinum electrocatalyst for the effective reduction of nitrate in a low conductive medium: Mechanism, adsorption thermodynamics and stability. *Appl. Catal. A Gen.* **478**, 259–266 (2014). <https://doi.org/10.1016/j.apcata.2014.04.017>
81. A.A. Ismail, F.A. Harraz, M. Faisal, A.M. El-Toni, A. Al-Hajry, M.S. Al-Assiri, A sensitive and selective amperometric hydrazine sensor based on mesoporous Au/ZnO nanocomposites. *Mater. Des.* **109**, 530–538 (2016). <https://doi.org/10.1016/j.matdes.2016.07.107>
82. C. Karupiah, S. Palanisamy, S.-M. Chen, S.K. Ramaraj, P. Periakaruppan, A novel and sensitive amperometric hydrazine sensor based on gold nanoparticles decorated graphite nanosheets modified screen printed carbon electrode. *Electrochim. Acta.* **139**, 157–164 (2014). <https://doi.org/10.1016/j.electacta.2014.06.158>
83. M. Khairy, R.O. Kadara, C.E. Banks, Electroanalytical sensing of nitrite at shallow recessed screen printed microelectrode arrays. *Anal. Methods.* **2**, 851–854 (2010). <https://doi.org/10.1039/C0AY00142B>
84. S. Li, J. Qu, Y. Wang, J. Qu, H. Wang, A novel electrochemical sensor based on carbon nanoparticle composite films for the determination of nitrite and hydrogen peroxide. *Anal. Methods.* **8**, 4204–4210 (2016). <https://doi.org/10.1039/C6AY00030D>
85. L. Sun, H. Li, M. Li, P. Li, C. Li, B. Yang, Simultaneous determination of small biomolecules and nitrite using an Au/TiO₂/carbon nanotube composite-modified electrode. *J. Electrochem. Soc.* **163**, B567–B572 (2016). <https://doi.org/10.1149/2.0361613jes>
86. J. Qu, Y. Dong, Y. Wang, T. Lou, X. Du, J. Qu, A novel nanofilm sensor based on poly-(alizarin red)/Fe₃O₄ magnetic nanoparticles-multiwalled carbon nanotubes composite material for determination of nitrite. *J. Nanosci. Nanotechnol.* **16**, 2731–2736 (2016). <https://doi.org/10.1166/jnn.2016.10763>
87. K. Promsuwan, P. Thavarungkul, P. Kanatharana, W. Limbut, Flow injection amperometric nitrite sensor based on silver microcubics-poly (acrylic acid)/poly (vinyl alcohol) modified screen printed carbon electrode. *Electrochim. Acta.* **232**, 357–369 (2017). <https://doi.org/10.1016/j.electacta.2017.02.138>
88. L. Liu, H. Cui, H. An, J. Zhai, Y. Pan, Electrochemical detection of aqueous nitrite based on poly(aniline-co-o-aminophenol)-modified glassy carbon electrode. *Ionics (Kiel).* **23**, 1517–1523 (2017). <https://doi.org/10.1007/s11581-017-1972-6>
89. M. Sivakumar, M. Sakthivel, S.M. Chen, K. Pandi, T.W. Chen, M.C. Yu, An electrochemical selective detection of nitrite sensor for polyaniline doped graphene oxide modified electrode. *Int. J. Electrochem. Sci.* **12**, 4835–4846 (2017). <https://doi.org/10.20964/2017.06.24>
90. Y. Zhang, F. Wen, J. Tan, C. Jiang, M. Zhu, Y. Chen, H. Wang, Highly efficient electrocatalytic oxidation of nitrite by electrodeposition of Au nanoparticles on molybdenum sulfide and multi-walled carbon nanotubes. *J. Electroanal. Chem.* **786**, 43–49 (2017). <https://doi.org/10.1016/j.jelechem.2017.01.007>

91. Y. Shen, G. Zhu, J. Yang, J. Liu, Ultrafine copper decorated polypyrrole nanotube electrode for nitrite detection. *Ionics (Kiel)*. **25**, 297–307 (2019). <https://doi.org/10.1007/s11581-018-2577-4>
92. Y. Tian, J. Wang, Z. Wang, S. Wang, Electroreduction of nitrite at an electrode modified with polypyrrole nanowires. *Synth. Met.* **143**, 309–313 (2004). <https://doi.org/10.1016/j.synthmet.2003.12.014>
93. C.-Y. Lin, V.S. Vasantha, K.-C. Ho, Detection of nitrite using poly(3,4-ethylenedioxythiophene) modified SPCEs. *Sensors Actuators B Chem.* **140**, 51–57 (2009). <https://doi.org/10.1016/j.snb.2009.04.047>
94. Y.D. Zhao, W.D. Zhang, Q.-M. Luo, S.F. Yau Li, The oxidation and reduction behavior of nitrite at carbon nanotube powder microelectrodes. *Microchem. J.* **75**, 189–198, (2003). [https://doi.org/10.1016/S0026-265X\(03\)00096-1](https://doi.org/10.1016/S0026-265X(03)00096-1)
95. W. Wang, J. Leng, Y. Yu, L. Lu, L. Bai, X. Qiu, An electropolymerized rhodamine b sensing film-based electrochemical sensor for nitrite with high sensitivity and selectivity. *Int. J. Electrochem. Sci.* **9**, 921–930 (2014)
96. Y. Zhang, P. Chen, F. Wen, C. Huang, H. Wang, Construction of polyaniline/molybdenum sulfide nanocomposite: characterization and its electrocatalytic performance on nitrite. *Ionics (Kiel)*. **22**, 1095–1102 (2016). <https://doi.org/10.1007/s11581-015-1634-5>

Publisher's Note Springer Nature remains neutral with regard to jurisdictional claims in published maps and institutional affiliations.